PAPER

Structural and magnetic properties of the $Yb_2Pd_2(In_{1-x}Sn_x)$ system: a synchrotron x-ray and neutron powder diffraction investigation

To cite this article: A Martinelli *et al* 2019 *J. Phys.: Condens. Matter* **31** 385802

IOP Publishing Journal of Physics: Condensed Matter
J. Phys.: Condens. Matter **31** (2019) 385802 (8pp) https://doi.org/10.1088/1361-648X/ab2b83

Structural and magnetic properties of the $Yb_2Pd_2(In_{1-x}Sn_x)$ system: a synchrotron x-ray and neutron powder diffraction investigation

A Martinelli[1], S Sanna[1,2], G Lamura[1], C Ritter[3], B Joseph[4], E Bauer[5] and M Giovannini[1,6]

[1] CNR-SPIN Corso Perrone 24, I-16152 Genova, Italy
[2] Dipartimento di Fisica e Astronomia, University of Bologna, via Berti-Pichat 6-2, I-40127 Bologna, Italy
[3] Institute Laue—Langevin, 6 rue Jules Horowitz, F-38042 Grenoble Cedex 9, France
[4] GdR IISc-ICTP, Elettra-Sincrotrone Trieste, S. S. 14 km 163.5, I-34149 Basovizza, Trieste, Italy
[5] Institute of Solid State Physics, Vienna University of Technology, 1040 Wien, Austria
[6] Dipartimento di Chimica e Chimica Industriale, University of Genova, Via Dodecaneso 31, I-16146 Genova, Italy

E-mail: alberto.martinelli@spin.cnr.it

Received 20 May 2019, revised 10 June 2019
Accepted for publication 20 June 2019
Published 8 July 2019

Abstract

The structural properties of the $Yb_2Pd_2(In_{1-x}Sn_x)$ system were investigated at room temperature by synchrotron x-ray powder diffraction. All the inspected compositions ($x = 0.0, 0.3, 0.4, 0.5, 0.6, 0.8, 0.9$) crystallize in the tetragonal space group *P*4/*mbm*; the cell parameters exhibit a non-linear dependence on composition, whereas cell volume changes more regularly, with a minimum at $x = 0.8$.

Samples with Sn content $x = 0.5, 0.6, 0.9$ were also analysed by neutron diffraction down to 0.5 K. No evidence for a structural transition can be detected at low temperature, whereas an antiferromagnetic ordering is observed, characterized by a propagation vectors $\mathbf{k} = (0,0,½)$. Magnetic moments order in the tetragonal *ab*-plane and the magnetic structure belongs to the Shubnikov magnetic space group *P*4/*mbm*.

Keywords: Yb_2Pd_2In, Yb_2Pd_2Sn, neutron diffraction, crystalline electric field effects, Rietveld refinement, magnetic structure

(Some figures may appear in colour only in the online journal)

1. Introduction

Strong correlations between electrons in rare earth intermetallic compounds, owing to the hybridization of conduction and *f*-electrons, can result in a number of anomalous low temperature properties like heavy fermion behaviour, intermediate valence or the Kondo effect. Especially Ce- and Yb-based compounds can show these interesting phenomena. Chemical composition, as well as magnetic field and pressure, can play a fundamental role in changing the ground state properties leading in some cases to quantum critical transitions between magnetic and non-magnetic ground states [1–5]. The class of compounds characterized by a nominal chemical composition RE_2T_2X (RE = rare earth; T = transition metal; X = In, Sn, Pb, Cd) exhibits a large variety of intriguing physical properties [6–10]. In particular, in a number of recent investigations, we explored the physical properties of RE_2Pd_2X (RE = Yb, Ce; X = In, Sn), crystallizing with the tetragonal Mo_2FeB_2

Table 1. Structural parameters of $Yb_2Pd_2(In_{1-x}Sn_x)$ samples, as refined from XRPD data collected at 300 K; space group *P*4/*mbm*, Yb is located at the 4*h* site (*x*,*x* + ½,½) site, Pd at the 4*g* site (*x*,*x* + ½,0) site, Sn and In at the 2*a* site (0,0,0).

	$x = 0.0$	$x = 0.3$	$x = 0.4$	$x = 0.6$	$x = 0.8$
a (Å)	7.5909(1)	7.5902(1)	7.5861(1)	7.5818(1)	7.5756(1)
c (Å)	3.6391(1)	3.6312(1)	3.6312(1)	3.6325(1)	3.6362(1)
x Yb	0.1716(1)	0.1722(1)	0.1722(1)	0.1724(1)	0.1724(1)
x Pd	0.6293(1)	0.6295(1)	0.6286(1)	0.6284(1)	0.6286(1)
R_{Bragg}	1.98	2.94	1.95	2.65	1.58
R_{factor}	1.09	2.38	0.94	1.41	0.73

structure-type, focusing on the conditions leading to the formation of magnetic ground states. In this class of compounds, antiferromagnetism is very common, although it can occur with different propagation vectors, whereas ferromagnetism is rarely observed [11]. In the case of Ce_2Pd_2In ferro- or antiferromagnetism can be selectively observed depending on slight changes in composition [12]. On the other hand, neither Yb_2Pd_2In nor Yb_2Pd_2Sn exhibit long-range magnetic order and both compounds show non-Fermi liquid behaviour at low temperatures [13, 14]. The application of pressure to Yb_2Pd_2Sn originates the formation of a magnetic dome from 10 to 40 kbar with the appearance of two quantum critical points [15, 16]. Noteworthy, a magnetic dome occurs also inside the Yb_2Pd_2(In,Sn) region, as shown by thermal and transport properties, and by a preliminary treatment of neutron scattering data [13, 14, 17].

In this work, using the combined probes of x-ray and neutron diffraction, we present a thorough investigation of structural properties and the antiferromagnetic ground state inside the magnetic dome of the Yb_2Pd_2(In,Sn) system.

2. Experimental

Samples pertaining to the $Yb_2Pd_2(In_{1-x}Sn_x)$ system with $x = 0.0, 0.3, 0.4, 0.5, 0.6, 0.8, 0.9$ were prepared from stoichiometric amounts of elements by high frequency melting the constituent materials in closed tantalum crucibles. A subsequent heat treatment at 1250 K for one week served to ensure phase purity.

Synchrotron x-ray powder diffraction (XRPD) analysis was carried out at 300 K at the x-ray diffraction beamline of Elettra (Trieste, Italy); data were collected at ambient pressure using a radiation wavelength $\lambda = 0.7000$ Å (samples with $x = 0.0, 0.3, 0.4, 0.6, 0.8$).

Neutron powder diffraction (NPD) was performed at the Institute Laue Langevin in Grenoble (France); diffraction patterns were collected in the thermal range 5.0 K ~ 0.5 K at the D1B beamline using a ^{3}He-cryostat ($\lambda = 2.520$ Å; samples $x = 0.1, 0.4, 0.5$).

Structural refinement was obtained according to the Rietveld method [18] using the program FullProf [19]; the following parameters were refined: the scale factor; the background; the zero point of the detector; the unit cell parameters; the atomic site coordinates not constrained by symmetry; the atomic displacement parameters.

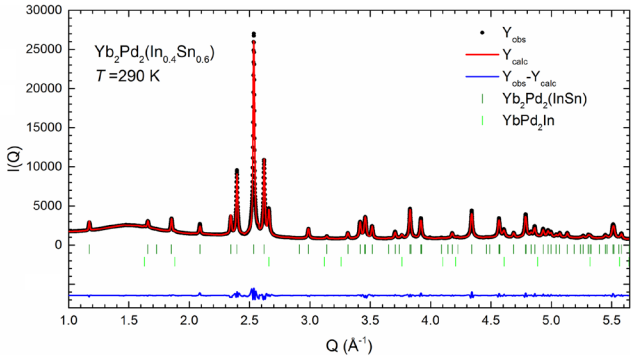

Figure 1. Rietveld refinement plot for $Yb_2Pd_2(In_{0.4}Sn_{0.6})$ (XRPD data collected at Xpress); in the upper field the continuous red line is the calculated fit superposed to the experimental intensity data (black points); the blue line in the lower field is the difference curve; the green vertical bars indicate Bragg reflections.

3. Results

3.1. Structural properties

At 300 K, all the analysed samples crystallize in the tetragonal space group *P*4/*mbm* and are isotypic with Mo_2FeB_2; no evidence for a structural transformation dependent on the Sn content can be detected. Table 1 lists the structural data obtained by Rietveld refinements using the XRPD data collected at 300 K at the Xpress beamline, whereas figure 1 shows the Rietveld refinement plot obtained for the sample $Yb_2Pd_2(In_{0.4}Sn_{0.6})$ selected as representative (a minor amount of $YbPd_2In$ can be also detected).

The cell parameters exhibit a non-linear dependence on composition, whereas cell volume changes more regularly, displaying a minimum around $x = 0.8$ (figure 2). These data are in a rather good agreement with those previously obtained on a similar $Yb_2Pd_2(In_{1-x}Sn_x)$ sample series [14]. As already pointed out by Bauer *et al* [14], the irregular evolution of the structural parameters with composition can be ascribed to different and competing effects, such as the different external electronic configurations, characterizing In and the substituting Sn; furthermore, the competition between magnetic and Kondo interactions and the variation of the valence state of the Yb ions. In particular, the trend with a minimum of the *c* parameter (which depends on Yb–Yb distance along the *c*-axis) is probably driven by the variation of valence of Yb-ion from 2.9 for both border compounds Yb_2Pd_2In and Yb_2Pd_2Sn to the value of 3 in the middle of the solid solution.

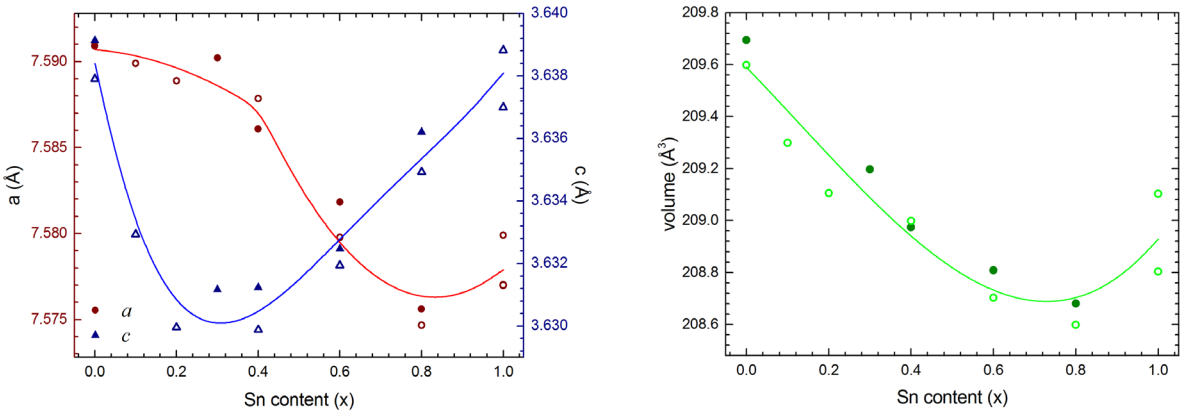

Figure 2. Dependence on Sn-content of the cell edges (panel on the left) and cell volume (panel on the right); full symbols: present study; open symbol: data from [14, 20]; lines are guides to the eye.

The comparison of the structural parameters measured for the different members of the $Yb_2Pd_2(In_{1-x}Sn_x)$ solid solution reveals the impact of the Sn-substitution on the crystal structure; as Sn is characterized by lower atomic radius than In, a structural compression is expected to occur after substitution. Figure 3 shows the evolution of the strain ellipsoids with composition; the dashed sphere is representative of the Yb_2Pd_2In structure, whereas ellipsoids depict the structural compression taking place with the increase of the Sn content (the eccentricity of the ellipsoids has been stressed to clearly represent the changes). Since that all the inspected compounds crystallize in the tetragonal system, the principal axes of the strain ellipsoids are parallel to the crystallographic a and c axes. Referreing to the parent compound Yb_2Pd_2In, the compression is anisotropic for all the inspected samples. The compressive strain along the a axis is negligible for the sample with $x = 0.3$, but then increases by increasing the Sn content, being maximum for $x = 0.8$. Conversely, the compressive strain along the c axis is maximum for the solid solution samples containing the lower amount of Sn ($x = 0.3$ and 0.4); as the Sn content is increased, the strain decreases.

This behavior can be explained by inspecting the atomic displacement patterns resulting from the Sn-substitution (figure 4). In fact, the composition $Yb_2Pd_2(In_{0.7}Sn_{0.3})$ displays a peculiar pattern, consistent with a negligible in-plane strain. In this case, all the in-plane displacements of the Yb atoms are compensated by similar displacements of the Pd atoms in the opposite direction; then the cell is only compressed along the c-axis on account of the lower size of the substituting Sn. Conversely, for the samples with $x = 0.4$–0.8, neighboring Yb and Pd atoms are in-plane displaced along the same directions within each unit cell, thus producing the in-plane structural strain.

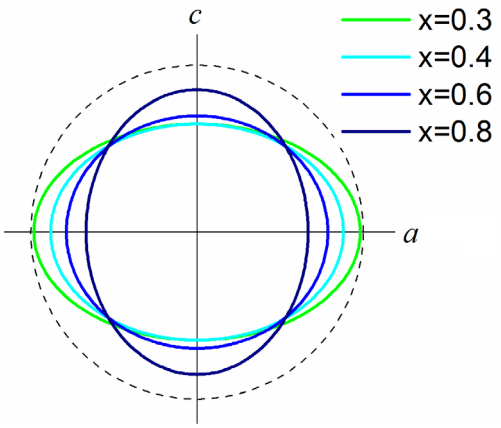

Figure 3. Strain ellipsoids for structural deformation obtained by increasing the Sn-content; for the sake of clarity, the eccentricity of the ellipsoids has been stressed.

3.2. Magnetic properties

Samples with Sn content $x = 0.5$, 0.6, 0.9 were also analysed by neutron diffraction down to 0.5 K. Rietveld refinements reveal that the inspected samples crystallize in the tetragonal *P4/mbm* space group down to 0.5 K (figure 5) and no evidence for any structural transformation is detected. For $T \leqslant 3.0$ K, neutron magnetic scattering is observed in the NPD data; the magnetic Bragg peaks can be successfully indexed according to the propagation vectors $\mathbf{k} = (0,0,½)$.

The symmetry allowed magnetic structures were calculated for the 4*h* site, where the magnetic atom Yb is located, using the program BasIreps [21, 22]. Table 2 lists the resulting 10 irreducible representation (*irrep*) of the little group $\mathbf{G_k}$ for $\mathbf{k} = (0,0,½)$; eight *irreps* are of dimension 1, whereas two *irreps* are of dimension 2. The magnetic representation Γ_m decomposes in terms of the *irreps* as $\Gamma_m(4h) = 1\ \Gamma_1 \oplus 1\ \Gamma_2 \oplus 1\ \Gamma_3 \oplus 1\ \Gamma_5 \oplus 1\ \Gamma_6 \oplus 1\ \Gamma_7 \oplus 2\ \Gamma_9 \oplus 1\ \Gamma_{10}$; as a consequence, 1 free parameter is needed if a single Γ_i describes the magnetic structure ($i = 1, 2, 3, 5, 6, 7$). Γ_9 and Γ_{10} have dimension 2 and are present twice and once in $\Gamma_m(4h)$, respectively, hence up to 4 and 2 parameters might be needed for their description (table 3).

The magnetic scattering contribution to the NPD pattern can be fitted by applying the *irrep* Γ_1 for $\mathbf{G_k}$ (tables 2 and 3) corresponding to an antiferromagnetic ordering at the Yb (4*h*) sub-structure with magnetic moments $\mathbf{m} = 0.81(1)\mu_B$ at 1.5 K (for $x = 0.5$) lying in the tetragonal *ab*-plane (figure 6). This magnetic structure belongs to the Shubnikov magnetic space group *P4/mbm* (magnetic space group number: 127.387).

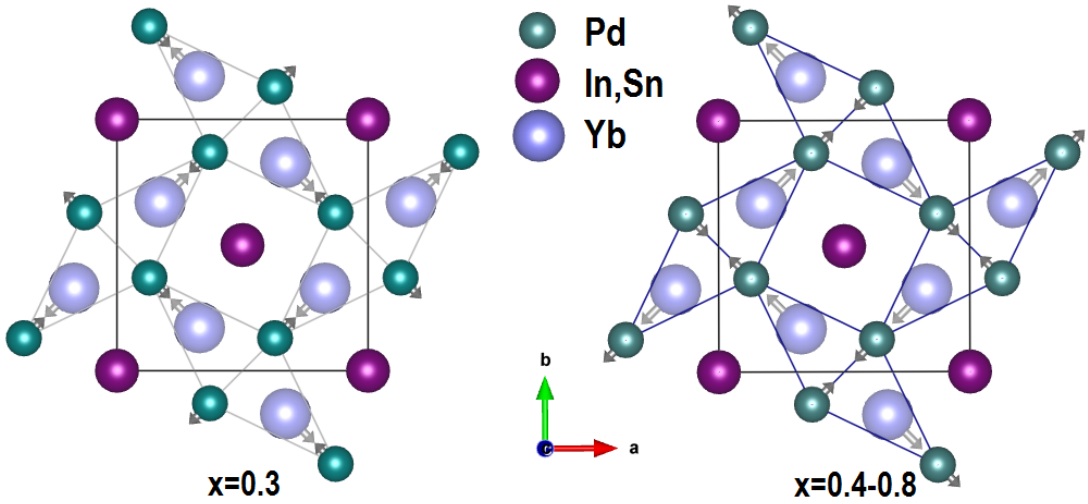

Figure 4. Atomic displacement patterns observed after Sn-substitution in $Yb_2Pd_2(In_{1-x}Sn_x)$ for $x = 0.3$ (on the left) and $x = 0.4$–0.8 (on the right).

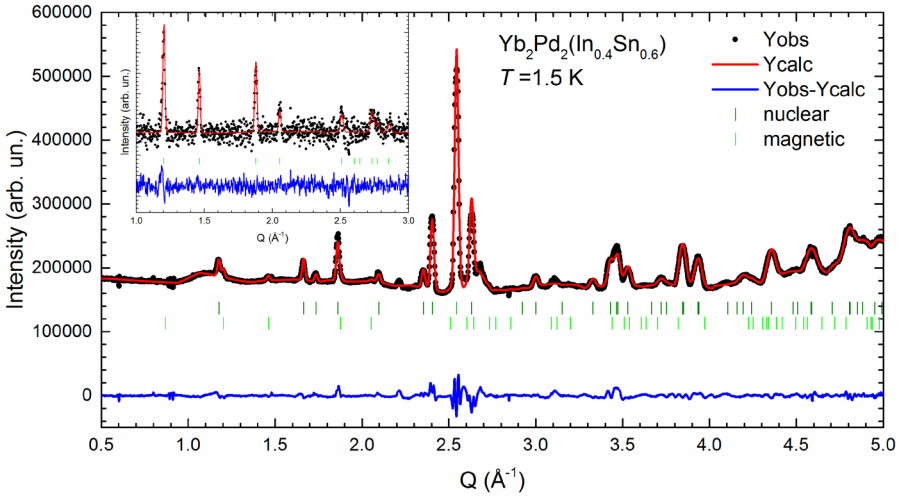

Figure 5. Rietveld refinement plot for $Yb_2Pd_2(In_{0.4}Sn_{0.6})$ (NPD data collected at 1.5 K); the inset shows a selected range of the fitted difference NPD pattern (1.5 K–4.5 K data).

The thermal dependence of the ordered magnetic moment **m** (figure 7) may be described using a simple power law:

$$m = m_0 \cdot (1 - T/T_m)^{\beta}.$$

Where T_m is the magnetic transition temperature, m_0 the magnetic moment at $T = 0$ K and β the critical exponent; for $x = 0.5$ and 0.6, T_m results in 2.64 K and 3.30 K, whereas $\beta = 0.41$ and 0.29, respectively. In particular the critical exponent values are consistent with those measured in the isotypic U_2Rh_2Sn, U_2Pt_2In and U_2Ni_2In compounds [23, 24].

These measurements demonstrate that magnetic ordering is induced by substitution; in particular the values of the refined magnetic moments, as well as those of T_m, attain a maximum for $x = 0.6$ (figure 7). Nonetheless, the measured magnetic moments are much lower than the theoretical effective magnetic moment expected for the Yb^{3+} ion (4.54 μ_B) in all the inspected compositions.

3.3. Magnetic structures of RE_2Pd_2In and RE_2Pd_2Sn compounds

At this point it is instructive to review the magnetic structures of both RE_2Pd_2In and RE_2Pd_2Sn compounds as obtained by neutron diffraction, in order to highlight similarities, differences and trends. Primarily, all these compounds are isotypic with Mo_2FeB_2; this property can be used to carry out a comparative investigation about the effect of the *RE* ion on the magnetic properties.

Ce_2Pd_2In is a non-stoichiometric compound allowing the development of two different solid solution branches on account of different substitutional mechanisms; in the Pd-rich branch the antiferromagnetic structure is characterized by an incommensurate magnetic propagation wave vector $\mathbf{k} = (\delta,0,0)$ whereas in the Ce-rich branch a ferromagnetic order is observed; in both cases magnetic moments are aligned parallel to the *c* axis [12]. As Pd is progressively

Table 2. Small irreducible representations of the little group $\mathbf{G_k}$ for $\mathbf{k} = (0,0,½)$.

Symmetry operations			Irrep											
			Γ_1	Γ_2	Γ_3	Γ_4	Γ_5	Γ_6	Γ_7	Γ_8	Γ_9		Γ_{10}	
x	y	z	1	1	1	1	1	1	1	1	1	0	1	0
											0	1	0	1
$-x$	$-y$	z	1	1	1	1	1	1	1	1	−1	0	−1	0
											0	−1	0	−1
$-x+½$	$y+½$	$-z$	1	1	1	1	−1	−1	−1	−1	1	0	1	0
											0	−1	0	−1
$x+½$	$-y+½$	$-z$	1	1	1	1	−1	−1	−1	−1	−1	0	−1	0
											0	1	0	1
$y+½$	$x+½$	$-z$	1	1	−1	−1	1	1	−1	−1	0	1	0	1
											1	0	1	0
$-y+½$	$-x+½$	$-z$	1	1	−1	−1	1	1	−1	−1	0	−1	0	−1
											−1	0	−1	0
y	$-x$	z	1	1	−1	−1	−1	−1	1	1	0	−1	0	−1
											1	0	1	0
$-y$	x	z	1	1	−1	−1	−1	−1	1	1	0	1	0	1
											−1	0	−1	0
$-x$	$-y$	$-z$	1	−1	1	−1	1	−1	1	−1	−1	0	1	0
											0	−1	0	1
x	y	$-z$	1	−1	1	−1	1	−1	1	−1	1	0	−1	0
											0	1	0	−1
$x+½$	$-y+½$	z	1	−1	1	−1	−1	1	−1	1	−1	0	1	0
											0	1	0	−1
$-x+½$	$y+½$	z	1	−1	1	−1	−1	1	−1	1	1	0	−1	0
											0	−1	0	1
$-y+½$	$-x+½$	z	1	−1	−1	1	1	−1	−1	1	0	−1	0	1
											−1	0	1	0
$-y+½$	$-x+½$	$-z$	1	−1	−1	1	1	−1	−1	−1	0	1	0	−1
											1	0	−1	0
$-y$	x	$-z$	1	−1	−1	1	−1	1	1	−1	0	1	0	−1
											−1	0	1	0
y	$-x$	$-z$	1	−1	−1	1	−1	1	1	−1	0	−1	0	1
											1	0	−1	0

substituted by Ag, the pristine ferromagnetic ordering is suppressed; for $Ce_2(Pd_{0.5}Ag_{0.5})_2In$ a different ferromagnetic arrangement is observed, with magnetic moments aligned along the *b* axis [25].

In Pr_2Pd_2In an antiferromagnetic ordering with $\mathbf{k} = (0,0,½)$ and moments oriented parallel to the *c* axis occurs below $T_m = 5.0(5)$ K, corresponding to the *irrep* Γ_{10} described in tables 2 and 3, whereas in Nd_2Pd_2In modulated antiferromagnetism takes place below $T_m = 7.5(5)$ K, characterized by a wave vector $\mathbf{k} = (¼,¼,0)$ and moments parallel to the *c* axis [11].

In Ce_2Pd_2Sn two magnetic transitions are observed, a first antiferromagnetic transition at $T_{m1} = 4.8(2)$ K, followed by a ferromagnetic transition at $T_{m2} = 3.0(2)$ K; the antiferromagnetic structure is incommensurate with $\mathbf{k_1} = (\delta,0,½)$ with magnetic moments aligned parallel to the *c* axis, as well as in the low temperature ferromagnetic structure [26].

The case of Tb_2Pd_2Sn is particularly interesting in our context. This compound displays two antiferromagnetic transitions at $T_{m1} = 27.3(2)$ K and $T_{m2} = 20.8(5)$ K; below T_{m1}, the magnetic structure is characterized by an incommensurate wave vector $\mathbf{k_1} = (\delta,\delta,½)$, with δ decreasing on cooling down to T_{m2} where the structure becomes commensurate with $\mathbf{k_2} = (0,0,½)$; moreover the Tb magnetic moments lie in the *ab* plane [27] according to the *irrep* Γ_9 listed in tables 2 and 3. Hence at low temperature both Tb_2Pd_2Sn and $Yb_2Pd_2(In_{1-x}Sn_x)$ are characterized by the same magnetic propagation vector and both display magnetic moments arranged in the *ab* plane. Nevertheless, the measured Tb^{3+} magnetic moments (8.70 μ_B) are close to the theoretical value (9.72 μ_B) [27], whereas those of Yb^{3+} are strongly suppressed. Concerning the crystal electric field effect, as pointed out by Laffargue *et al* [27], the site symmetry of the 4*h* site, where the *RE* ions are located is *m*.2*m* with one mirror plane perpendicular to the *c* axis and the other perpendicular to the general direction $\langle 1\,1\,0\rangle$, this latter being the easy magnetic axis as actually observed in both Tb_2Pd_2Sn and $Yb_2Pd_2(In_{1-x}Sn_x)$ compounds. As afore mentioned, in Tb_2Pd_2Sn the measured value of the magnetic moment is close to the theoretical one and hence the effect of the crystal electric field splitting is almost negligible. Conversely, in the

Table 3. Fourier coefficients obtained from the basis vectors for the different coordinates of the 4*h* site; *u*, *v*, *p*, *w* represent the free parameters of the possible magnetic structures.

Site 4*h*			Γ_1			Γ_2			Γ_3			Γ_5			Γ_6			Γ_7			Γ_9			Γ_{10}		
x	*y*	*z*	*x*	*y*	*z*	*x*	*y*	*z*	*x*	*y*	*z*	*x*	*y*	*z*	*x*	*y*	*z*	*x*	*y*	*z*	*x*	*y*	*z*	*x*	*y*	*z*
x	$x+½$	½	*u*	$-u$	0	0	0	*u*	*u*	*u*	0	*u*	$-u$	0	0	0	*u*	*u*	*u*	0	$u-p$	$v-w$	0	0	0	$u+v$
$-x$	$-x+½$	½	$-u$	*u*	0	0	0	*u*	$-u$	$-u$	0	$-u$	*u*	0	0	0	*u*	$-u$	$-u$	0	$u-p$	$v-w$	0	0	0	$-u-v$
$-x+½$	*x*	½	*u*	*u*	0	0	0	*u*	*u*	$-u$	0	$-u$	$-u$	0	0	0	$-u$	$-u$	*u*	0	$u+p$	$-v-w$	0	0	0	$u-v$
$x+½$	$-x$	½	$-u$	$-u$	0	0	0	*u*	$-u$	*u*	0	*u*	*u*	0	0	0	$-u$	*u*	$-u$	0	$u+p$	$-v-w$	0	0	0	$-u+v$

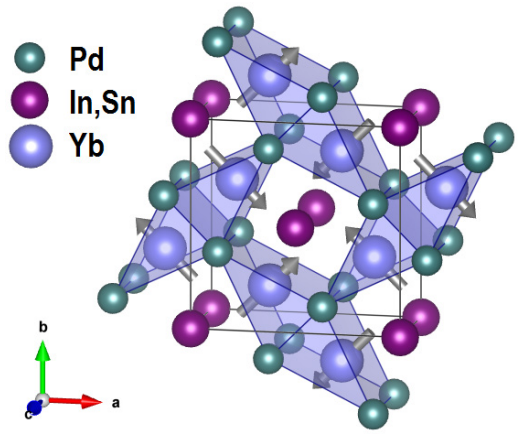

Figure 6. Crystal structure and magnetic moments ordering of $Yb_2Pd_2(In_{0.4}Sn_{0.6})$.

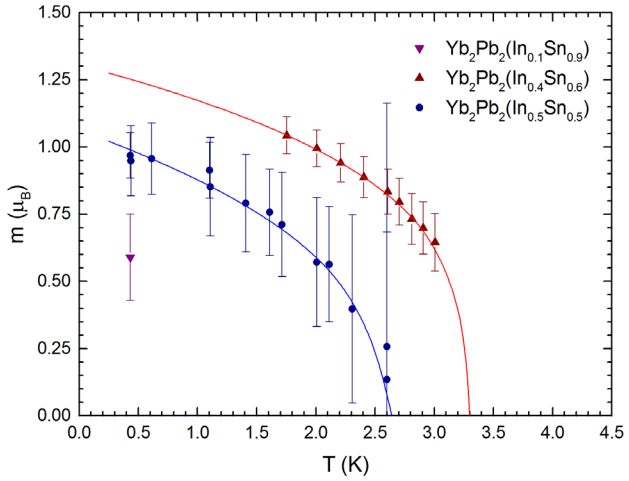

Figure 7. Thermal dependence of the ordered magnetic moment at the Yb sub-structure in $Yb_2Pd_2(In_{1-x}Sn_x)$; the solid lines represent the best fits.

inspected $Yb_2Pd_2(In_{1-x}Sn_x)$ series the experimental value of the magnetic moment is strongly reduced; hence, it can be argued that in this case the crystal electric field splitting might play a significant role.

Expanding this review to the whole class of compounds isotypic with Mo_2FeB_2, several other phases are characterized by an antiferromagnetic structure with wave vector $\mathbf{k} = (0,0,½)$ (see tables 2 and 3 [28]); U_2Ni_2In orders according to the *irrep* Γ_7, U_2Ni_2Sn with *irrep* Γ_9 [29] (as the afore mentioned Tb_2Pd_2Sn compound), $U_2Pd_{2.35}Sn_{0.65}$ with *irrep* Γ_2 [30] and U_2Rh_2Sn with *irrep* Γ_6 [23]. Note that all these compounds are U-bearing stannides.

Discussion and conclusions

Although the concentration of the Yb magnetic ions in $Yb_2Pd_2(In,Sn)$ does not change, there is a significant variation of both the ordering temperature as well as of the ordered moments. This indicates that the In/Sn substitution substantially modifies electronic features around the Fermi energy due to the increase of the valence electron count. Obviously, there is also a non-monotonic change of the unit cell volume. This refers to a non-monotonic variation of chemical pressure as well, being largest for samples away from $x = 0.0$ and $x = 1.0$ (end-member compositions). It is well known that pressure exerted to Yb systems responses oppositely to Ce ones, strengthening the magnetic $4f^{13}$ electronic configuration and weakening the Kondo effect. As a consequence, long-range magnetic order occurs for Sn substituted samples, but is absent in both Yb_2Pd_2In and Yb_2Pd_2Sn. The very distinct features regarding the ordered moment and the magnetic phase transition temperature is the result of a subtle balance from the crystalline electric field (CEF) ground state, from the RKKY and the Kondo interaction strength. In an earlier study we have shown that CEF effects are large in the case of Yb_2Pd_2In, with an overall splitting of about 49 meV and a CEF ground state doublet, well separated from the first excited level [14]. No such data are available in the case of Yb_2Pd_2Sn. Mössbauer measurements down to 40 mK, however, demonstrate that the ground states of both systems is non-magnetic, but distinctly different [14, 15]. The non-monotonous evolution of the long-range magnetic order and of the ordered moment is then a balance of the RKKY interaction (T_{RKKY}) and of the Kondo effect (T_K). In general, if $T_{RKKY} > T_K$, the system orders magnetically, whereas does not show magnetic order in the opposite case. Magnetic ordering is non-monotonous due to of the non-monotonous variation of chemical pressure onto the Yb ions throughout the series. This quite unique scenario becomes additionally complicated and overlaid from the evolution of the specific ground state, when proceeding from Yb_2Pd_2In to Yb_2Pd_2Sn. The CEF ground state of both ternary Yb compounds is still unknown. The magnitude of the ordered moment (~ 1 μ_B) deduced from the present elastic neutron scattering measurements, which is well below the moment of a free Yb^{3+} ion ($m_{Yb} = g_j\{J(J+1)\}^{½} = 4.54$ μ_B with $g_j = 8/7$ and $J = 7/2$) is reasonably well described by the resultant ground state doublet, consisting of a linear combination of $|\pm 1/2>$ to $|\pm 7/2>$ states. Note, a predominant $|\pm 1/2>$ would just yield a moment of just 0.57 μ_B.

In conclusion, the structural and magnetic properties characterizing the $Yb_2Pd_2(In_{1-x}Sn_x)$ system were investigated by x-ray and neutron powder diffraction. The compounds crystallize in the tetragonal space group *P4/mbm* in the whole thermal and compositional range; cell parameters are characterized by a non-linear dependence on composition, whereas cell volume changes more regularly. At low temperature, antiferromagnetic order appears in the middle of the In/Sn substitution with magnetic propagation wave vector $\mathbf{k} = (0,0,½)$ with moments arranged in the *ab* plane. The values of the ordered magnetic moment and the magnetic transition temperature depend on the Sn-content, being maximum for $x = 0.6$. Importantly, the magnitude of the experimental ordered moment is strongly suppressed by crystalline electric field effects in all the inspected compositions, being much lower than the theoretical 4.54 μ_B expected for free Yb^{3+} ion.

Acknowledgments

BJ acknowledges IISc Bangalore and ICTP Trieste for support through an IISc-ICTP fellowship.

ORCID iDs

A Martinelli https://orcid.org/0000-0001-8391-3486
S Sanna https://orcid.org/0000-0002-4077-5076
B Joseph https://orcid.org/0000-0002-3334-7540

References

[1] Gegenwart P, Si Q and Steglich F 2008 *Nat. Phys.* **4** 186
[2] von Löhneysen H, Rosch A, Vojta M and Wölfle P 2007 *Rev. Mod. Phys.* **79** 1015
[3] Custers J, Gegenwart P, Wilhelm H, Neumaier K, Tokiwa Y, Trovarelli O, Geibel C, Steglich F, Pépin C and Coleman P 2003 *Nature* **424** 524
[4] Carretta P, Pasero R, Giovannini M and Baines C 2009 *Phys. Rev.* B **79** 020401
[5] Carretta P, Giovannini M, Horvatic M, Papinutto N and Rigamonti A 2003 *Phys. Rev.* B **68** 220404
[6] Kaczorowski D, Rogl P and Hiebl K 1996 *Phys. Rev.* B **54** 9891
[7] Dhar S K, Settai R, nuki Y, Galatanu A, Haga Y, Manfrinetti P and Pani M 2007 *J. Magn. Magn. Mater.* **308** 143
[8] Kim M S and Aronson M C 2013 *Phys. Rev. Lett.* **110** 017201
[9] Sereni J G, G-Berisso M, Braghta A, Schmeber G and Kappler J P 2009 *Phys. Rev.* B **80** 024428
[10] Sereni J G, Giovannini M, Gomez Berisso M and Saccone A 2011 *Phys. Rev.* B **83** 064419
[11] Fischer P, Hermanndörfer T, Bonelli T, Fauth F, Keller L, Bauer E and Giovannini M 2000 *J. Phys.: Condens. Matter* **12** 7089
[12] Giovannini M *et al* 2000 *Phys. Rev.* B **61** 4044
[13] Bauer E, Hilscher G, Michor H, Paul Ch, Aoki Y, Sato H, Giovannini M and Saccone A 2004 *J. Magn. Magn. Mater.* **272–6** 237
[14] Bauer E *et al* 2005 *J. Phys.: Condens. Matter* **17** S999
[15] Muramatsu T *et al* 2011 *Phys. Rev.* B **83** 180404
[16] Yamaoka H *et al* 2017 *Sci. Rep.* **7** 5846
[17] Bauer E, Khan R T, Giovannini M and Ritter C 2010 *Phys. Status Solidi* b **247** 717
[18] Young R A 1993 The rietveld method *IUCr Monographs on Crystallography* vol 5, ed R A Young (Oxford: Oxford University Press) ch 1, p 1–38
[19] Rodríguez-Carvajal J 1993 *Physica* B **192** 55
[20] Giovannini M, Pasero R and Saccone A 2010 *Intermet* **18** 429
[21] Rodriguez-Carvajal J 2019 BASIREPS: a program for calculating irreducible representations of space groups and basis functions for axial and polar vector properties. Part of the FullProf Suite of programs (http://ill.eu/sites/fullprof/)
[22] Ritter C 2011 *Solid State Phenom.* **170** 263
[23] Pereira L C J, Paixao J A, Estrela P, Godinho M, Boudarot F, Bonnet M, Rebizant J, Spirlet J C and Almeida M 1966 *J. Phys.: Condens. Matter* **8** 11167
[24] Martin-Martin A, Pereira L C J, Lander G H, Rebizant J, Wastin F, Spirlet J C, Dervenagas P and Brown P J 1999 *Phys. Rev.* B **59** 11818
[25] Martinelli A, Giovannini M, Sereni J G and Ritter C 2018 *J. Phys.: Condens. Matter* **30** 265601
[26] Laffargue D, Fourgeot F, Bourèe F, Chevalier B, Roisnel T and Etourneau J 1996 *Solid State Commun.* **100** 575
[27] Laffargue D, Roisnel T, Chevalier B and Bourèe F 1997 *J. Alloys Compd.* **262–3** 219
[28] Tran V H, Zolnierek Z, Bourèe F and Roisnel T 1996 *J. Magn. Magn. Mater.* **161** 270
[29] Bourée F, Chevalier B, Fournès L, Mirambet F, Roisnel T, Tran V H and Zolnierek Z 1994 *J. Magn. Magn. Mater.* **138** 307
[30] Laffargue D, Bourée F, Chevalier B, Roisnel T, Gravereau P and Etourneau J 1997 *J. Magn. Magn. Mater.* **170** 155